communications materials

ARTICLE

https://doi.org/10.1038/s43246-022-00304-9 OPEN

Design and integration of single-qubit rotations and two-qubit gates in silicon above one Kelvin

Luca Petit[1], Maximilian Russ[1], Gertjan H. G. J. Eenink[1], William I. L. Lawrie[1], James S. Clarke[2], Lieven M. K. Vandersypen[1] & Menno Veldhorst[1✉]

Spin qubits in quantum dots define an attractive platform for quantum information because of their compatibility with semiconductor manufacturing, their long coherence times, and the ability to operate above one Kelvin. However, despite demonstrations of SWAP oscillations, the integration of this two-qubit gate together with single-qubit control to create a universal gate set as originally proposed for single spins in quantum dots has remained elusive. Here, we show that we can overcome these limitations and execute a multitude of native two-qubit gates, together with single-qubit control, in a single device, reducing the operation overhead to perform quantum algorithms. We demonstrate single-qubit rotations, together with the two-qubit gates CROT, CPHASE, and SWAP, on a silicon double quantum dot. Furthermore, we introduce adiabatic and diabatic composite sequences that allow the execution of CPHASE and SWAP gates on the same device, despite the finite Zeeman energy difference. Both two-qubit gates can be executed in less than 100 ns and, by theoretically analyzing the experimental noise sources, we predict control fidelities exceeding 99%, even for operation above one Kelvin.

[1] QuTech and Kavli Institute of Nanoscience, Delft University of Technology, PO Box 5046, 2600 GA Delft, The Netherlands. [2] Components Research, Intel Corporation, 2501 NE Century Blvd, Hillsboro, OR 97124, USA. ✉email: m.veldhorst@tudelft.nl

Two-qubit gates are at the heart of quantum information science, as they may be used to create entangled states with a complexity beyond what is classically simulatable[1], and ultimately may enable the execution of practically relevant quantum algorithms[2]. Optimizing two-qubit gates is therefore a central aspect across all qubit platforms[3]. In quantum dot systems, two-qubit gates can be naturally implemented using the exchange interaction between spin qubits in neighboring quantum dots[4]. Pulsing the interaction drives SWAP oscillations, where the spin states in the quantum dots are being exchanged, when the exchange energy is much larger than the Zeeman energy difference of the qubits[4–6], while it results in controlled-phase (CPHASE) oscillations, where only the phase information is exchanged, when the Zeeman energy difference is much larger than the exchange energy[7]. Single-qubit gates need also to be implemented to access the full two-qubit Hilbert space, and this requires distinguishability between the qubits. This is commonly obtained through the spin-orbit coupling[8,9] or by integrating nanomagnets[10,11], causing significant Zeeman energy differences. Realizing a high-fidelity SWAP-gate in this scenario would require extremely large values of exchange interaction. For this reason, the CPHASE operation has been the native gate in experimental demonstrations of two-qubit logic when the exchange interaction is pulsed[12–14]. An alternative implementation of two-qubit logic can be realized by driven rotations, which become state dependent in the presence of exchange interaction and can be used to realize controlled-rotation (CROT) operations[15–19]. Driving rotations can also be used to realize a resonant SWAP gate[20], which can be used to perform state swapping. While universal quantum logic can be obtained by combinations of single-qubit rotations and an entangling two-qubit operation[21], the ability to directly execute a multitude of two-qubit gates would reduce the number of operations required to execute practical algorithms.

Here, we demonstrate on the same device the implementation of the CROT, SWAP, and CPHASE, which are all essential gates in quantum computing and error correction applications. SWAP operations can in particular be useful in large quantum dot arrays, providing a mean to achieve beyond nearest-neighbor connectivity. We overcome the limitations imposed by the finite Zeeman energy difference between the qubits by introducing control sequences, which also allows the execution of the CPHASE and the SWAP in short time scales and a predicted high-fidelity. Moreover, we demonstrate these operations at temperatures exceeding one Kelvin. The cooling power at these elevated temperatures is much larger and thereby more compatible with the operation of classical electronics, such that quantum integrated circuits based on standard semiconductor technology become feasible[22–24].

Results and discussion

Silicon quantum dot device. The experimental two-qubit system is based on electron spin states confined in a silicon double quantum dot as schematically shown in Fig. 1a. The silicon double quantum dot is fabricated using an overlapping gate architecture on a silicon wafer with an isotopically enriched ^{28}Si epilayer of 800 ppm residual concentration of ^{29}Si[19,25]. In order to obtain an optimal exchange coupling between the electrons, qubits Q1 and Q2 are defined with $N_{Q1} = 1$ and $N_{Q2} = 5$, where N is the charge occupancy. Spin readout is performed at the (1,5)-(2,4) charge anticrossing, where the $|\uparrow\downarrow\rangle$ tunnels to the singlet (2,4) charge state, while the other sp in states are blocked because of the Pauli exclusion principle. By using an adiabatic pulse from the (2,4) to the (1,5) region, we initialize the system in the $|\downarrow\uparrow\rangle$ state. Because of the limited sensitivity of the single-electron-transistor (SET) that we use for charge readout, we average the single-shot readout traces and subtract a reference signal.

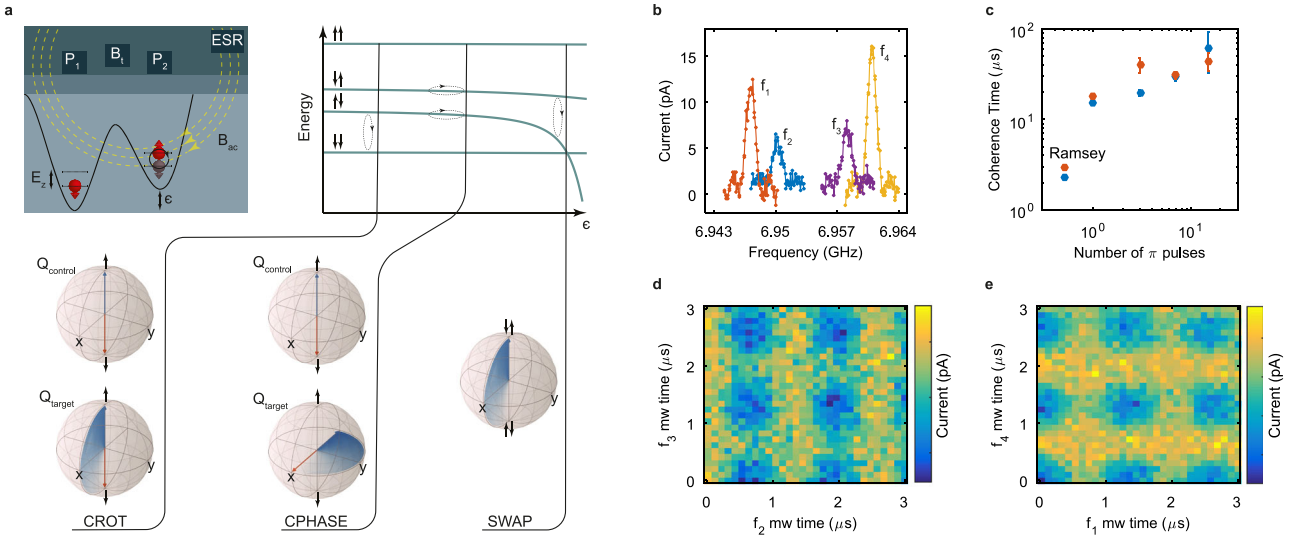

Fig. 1 Two-qubit gates and quantum coherence of silicon spin qubits operated at a $T = 1.05$ K. a Schematic representation of the double quantum dot system. The device is the same as used in ref. [19]. Two plunger gates (P_1 and P_2) and one barrier gate (B_t) are used to control the detuning energy ϵ and the tunnel coupling t between the quantum dots. Spin manipulation occurs via electron-spin-resonance (ESR) using an on-chip microwave line. The energy diagram displays the four electron spin states as a function of ϵ. We exploit both driven rotations and pulsed exchange for coherent control. Controlled rotations (CROTs) can in principle be executed at all points where $J \neq 0$, given that gate times are appropriately set. CPHASE gates are conveniently executed when the exchange interaction is much smaller than the Zeeman energy difference between the qubits, while SWAP oscillations can be realized when the exchange interaction is much larger. **b** Using ESR control we find the four resonance frequencies of the two-qubit system. Here, the exchange interaction is tuned to 3 MHz. The spectrum is composed of the frequencies: f_1 ($|\uparrow\downarrow\rangle \longrightarrow |\downarrow\downarrow\rangle$), f_2 ($|\downarrow\downarrow\rangle \longrightarrow |\downarrow\uparrow\rangle$), f_3 ($|\uparrow\uparrow\rangle \longrightarrow |\downarrow\uparrow\rangle$) and f_4 ($|\uparrow\downarrow\rangle \longrightarrow |\uparrow\uparrow\rangle$). **c** Coherence times as a function of the number of refocusing π pulses. Here, the exchange is set to 2 MHz. The plot includes the dephasing times measured through a Ramsey experiment to allow comparison. **d**, **e** Realization of CROT operations. Rabi oscillations of the target qubit are controlled by the spin state of the control qubit. We find controlled rotations on all the four resonance frequencies f_1, f_2, f_3, f_4.

We therefore obtain a current signal, proportional to the probability to have a blocked state. More details about the readout scheme can be found in ref. [19]. We note that the readout fidelity can be further improved, even at these higher temperatures[26], but here we focus on the coherent control (details on the reconstruction are in Supplementary Note 1: Reconstruction of the spin state probabilities). We perform spin manipulation via electron spin resonance (ESR) using an on-chip aluminum microwave antenna. All measurements have been performed in a dilution refrigerator at a temperature of $T_{\mathrm{fridge}} = 1.05$ K and with an external magnetic field of $B_{\mathrm{ext}} = 250$ mT.

Readout on Pauli spin blockade is relatively insensitive to temperature, since it does not rely on any external reservoir. However, a finite temperature can still affect qubit readout in the form of an enhanced relaxation[27]. Furthermore, the initialization fidelity can also be lowered due to a non zero population of the excited valley states in the (2,4) charge configuration. By taking into account the two singlet and the three triplet states and estimating a valley splitting of $E_{\mathrm{vs}} = 300$ μeV from previous works[19,27], we compute a total population of the ground singlet (2,4) charge state of 87%. This initialization fidelity can be pushed beyond 99% with a valley splitting $E_{\mathrm{vs}} > 550$ μeV (see Supplementary Note 2: Temperature effects on readout and initialization). Similar valley splitting values have already been measured in Si-MOS samples[9].

Qubit characterization. We control the exchange interaction J via the detuning ϵ between the two quantum dots and we measure couplings from $J = 2$ MHz up to $J = 45$ MHz, as shown in Supplementary Fig. 1a. By fitting the exchange spectrum we extract a Zeeman energy difference between the two qubits $\Delta E_z = 11$ MHz, which originates from the electron g-factor variations due to spin orbit coupling. This frequency difference is large enough to have a negligible impact on qubit control fidelities. The fitting suggests a negligible dependence of ΔE_z on detuning, further supported by the small magnetic field applied and the absence of external magnetic gradients. Figure 1b shows the four resonance frequencies of the two-qubit system when $J = 3$ MHz. At this value of exchange interaction we tune the π-rotation times to be $t_{\mathrm{CROT}} = 660$ ns such that we synchronize the Rabi oscillations of the target transition with the closest off-resonant transition in order to suppress crosstalk[28]. From Ramsey experiments on frequencies f_1 and f_4 we measure dephasing times $T^*_{2,\mathrm{Q1}} = 2.3$ μs and $T^*_{2,\mathrm{Q2}} = 2.9$ μs. The Carr-Purcell-Meiboom-Gill pulse sequence can extend the coherence times, by filtering out the low frequency noise. As shown in Fig. 1c, we measure a maximum $T_{2,\mathrm{Q1}} = 63$ μs and $T_{2,\mathrm{Q2}} = 44$ μs when 15 refocusing pulses are applied, setting benchmarks for the coherence time of quantum dot spin qubits at temperatures above one Kelvin.

When the exchange interaction is set to a non-zero value, it is possible to realize the CROT via driven rotations since the resonance frequency of one qubit depends on the state of the other qubit. This CROT gate is a universal two-qubit gate and equivalent to a CNOT gate up to single qubit phases[19]. Figure 1d, e shows controlled rotations by setting both configurations of target and control qubits.

Hot, fast, and high-fidelity CPHASE gates. An alternative way to achieve a universal gate set is through the implementation of the CPHASE gate. Moving in detuning energy toward the (1,5)-(2,4) charge anticrossing lowers the energy of the antiparallel $|\downarrow\uparrow\rangle$ and $|\uparrow\downarrow\rangle$ states with respect to the parallel $|\downarrow\downarrow\rangle$ and $|\uparrow\uparrow\rangle$ spin states. Therefore, pulsing the detuning for a time t results in a phase gate on the target qubit conditional on the spin state of the control qubit. When the total phase $\phi = \phi_{|\downarrow\uparrow\rangle} + \phi_{|\uparrow\downarrow\rangle} = (2n+1)\pi$ with n integer, a CPHASE gate is realized[7]. A high-fidelity implementation of such a gate requires a Zeeman energy difference between the two qubits much larger than the exchange interaction, in order to suppress the evolution of the exchange gate[4]. This condition is conveniently met in devices with micromagnets[13–15], where the CPHASE is the most natural choice as native two-qubit gate.

In our system, ΔE_z is comparable in magnitude to the accessible J (see Supplementary Note 3: Exchange spectrum), due to the small B_{ext} applied. This means that a detuning pulse will also cause the $|\downarrow\uparrow\rangle$ and $|\uparrow\downarrow\rangle$ states to undergo SWAP rotations. While these rotations occur along a tilted angle due to the non-zero ΔE_z, they can still reduce the fidelity of the CPHASE gate. In order to avoid unwanted SWAP rotations we implement an adiabatic detuning pulse, by ramping ϵ to the desired value instead of changing it instantaneously (see schematic in Fig. 2j). In this way, a high-fidelity CPHASE gate can still be realized with an arbitrarily small ΔE_z at the cost of a longer gate time. In Fig. 2a–f we change the duration of a detuning pulse in between a Ramsey-like experiment on Q1, with and without a π pulse applied to Q2. The frequency of the oscillations of Q1 depends strongly on the spin state of Q2, thereby demonstrating a controlled phase operation. Because of the finite Zeeman energy difference, the antiparallel $|\downarrow\uparrow\rangle$ state shifts significantly more in energy than the $|\uparrow\downarrow\rangle$ state. Consequently, the oscillations in Fig. 2c are significantly faster than in Fig. 2f. Similarly, the decay time in Fig. 2e is significantly longer than in Fig. 2b because of the lower sensitivity to electrical noise. In Fig. 2g–i the pulse time is calibrated such that the total phase $\phi = 3\pi$. We measure this in a Ramsey-like experiment where we probe the phase acquired by the target qubit for different control qubit states. From Fig. 2h, i, we can observe that the resulting oscillations are nicely out-of-phase, which demonstrates the CPHASE gate. We achieve a gate time $t_{\mathrm{CPHASE}} = 152$ ns, which is mostly limited by the adiabatic ramps which take $t_r = 60$ ns. From a comparison with simulations, we find that the contribution of both ramps to the total phase ϕ is approximately 1.7π.

This gate time can be significantly sped up with the implementation of a geometric CPHASE gate, that does not require adiabaticity[29]. For the implementation of this gate we synchronize the unwanted exchange oscillations with the total gate duration, i.e., our gate performs a CPHASE evolution while the exchange oscillations performs a complete cycle. For a perfectly diabatic pulse the condition for the exchange interaction is:

$$J = (4J_{\mathrm{res}} + \sqrt{3\Delta E_z^2 + 4J_{\mathrm{res}}^2})/3, \quad (1)$$

where J_{res} is the residual exchange interaction at the point where we perform CROT gates (see Supplementary Note 4: Two-qubit gate simulations).

Figure 2k, l shows the experimental implementation of the geometric CPHASE gate. We sweep the amplitude of the detuning pulse and monitor the spin state probabilities (see Supplementary Note 1: Reconstruction of the spin state probabilities) during exchange oscillations, and the total phase acquired by the antiparallel spin states. We notice that, when $\epsilon \approx 68$ mV, the antiparallel spin states execute a 2π rotation, while acquiring a total phase shift of π. At this value of detuning we measure $J \approx 10$ MHz (see Supplementary Note 3: Exchange spectrum) and therefore in agreement with Eq. (1). The total gate time is reduced here to $t_{\mathrm{CPHASE}} = 67$ ns.

Hot, fast, and high-fidelity SWAP operation. We now turn to the implementation of a SWAP gate, the originally proposed

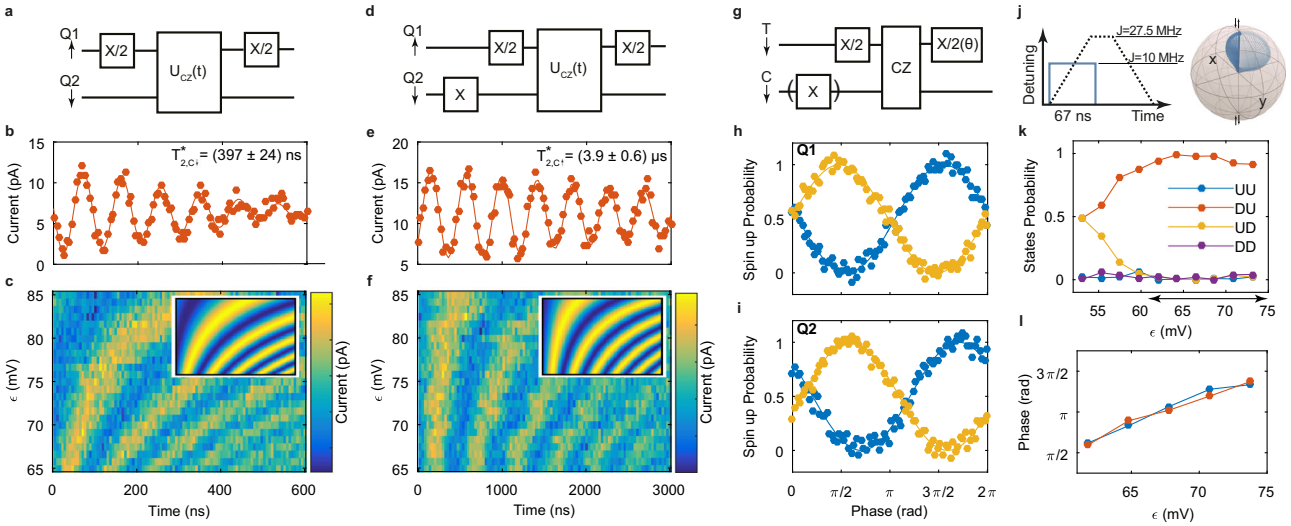

Fig. 2 Adiabatic and diabatic CPHASE operation at $T = 1.05$ K. Conditional phase oscillations (**b**, **c**, **e**, **f**) by adiabatically pulsing the detuning energy ϵ to increase the exchange interaction J, measured using the quantum circuit in **a**, **d**. The antiparallel spin states acquire a phase with respect to the parallel states, resulting in coherent oscillations as a function of the duration of the detuning pulse. At smaller detuning values, the exchange interaction increases resulting in faster oscillations. Due to the exchange interaction, the energy difference $E_{\downarrow\uparrow} - E_{\downarrow\downarrow}$ (measured in **b**, **c**) is smaller than $E_{\uparrow\uparrow} - E_{\uparrow\downarrow}$ (measured in **e**, **f**), resulting in an acquired phase on the target qubit (T) that is dependent on the state of the control qubit (C). **g** Schematic of the quantum circuit to verify CPHASE operation. The adiabatic detuning pulse of the CPHASE gate is tuned such that the antiparallel spin states acquire a total phase of 3π. The exchange is increased to $J = 27.5$ MHz using a ramp $t_r = 60$ ns and the total gate time is $t_{\mathrm{CPHASE}} = 152$ ns. **h**, **i** We verify CPHASE operation by measuring the normalized spin-up probability, obtained through conversion of the readout current, and observe clear antiparallel oscillations. **j** Schematic representation of an adiabatic (dashed black and shown in **g**–**i** and a diabatic (solid blue) CPHASE. **k** The diabatic CPHASE is optimized by changing the amplitude of ϵ and measuring probabilities of the four possible spin states. **k**, **l** The finite Zeeman difference ($\Delta E_z = 11$ MHz) results in SWAP-interactions that are not negligible. However, the exchange can be tuned such that the states undergo rotations of 2π. We tune and optimize this by measuring the phase, projected to the spin states through a π/2-pulse on the target qubit. We obtain a diabatic CPHASE for $t_{\mathrm{CPHASE}} = 67$ ns.

quantum gate for quantum dots[4]. Despite the experimental demonstration of exchange oscillations[5,6,30], its implementation together with single-qubit gates is rather challenging because of the requirement of a negligible Zeeman difference between the qubits. In the following we will discuss a protocol that can overcome this problem and allow for a high-fidelity SWAP gate, even in the presence of a finite ΔE_z.

In order to observe SWAP oscillations, we implement a sequence where we initialize in the $|\downarrow\uparrow\rangle$ state and pulse ϵ for a time t. Clear exchange oscillations between the $|\downarrow\uparrow\rangle$ and the $|\uparrow\downarrow\rangle$ state are visible when the detuning pulse is diabatic (see Fig. 3a, b), where the oscillation frequency is $f_{\mathrm{SWAP}} = \sqrt{J^2 + \Delta E_z^2}$. As we make the pulse more adiabatic by ramping ϵ, the oscillations disappear and the regime becomes suitable for a CPHASE implementation as discussed before. Even when the detuning pulse is perfectly diabatic, we do not obtain a perfect SWAP due to the finite ΔE_z. Instead, the spin states rotate in the Bloch sphere around the tilted axis of rotation $\boldsymbol{r} = (J, 0, \Delta E_z)^T$, similar to what happens for off-resonant driving. Figure 3c, d show that when starting in the $|\downarrow\uparrow\rangle$ state, a maximum $|\uparrow\downarrow\rangle$ state probability of 64% is obtained in $t_{\mathrm{SWAP}} = 18$ ns, which is in agreement with our simulated predictions (see Supplementary Note 4: Two-qubit gate simulations).

Composite pulse sequences[31,32] can correct for the tilted axis of rotation. It is possible to achieve full population transfer with an exchange sequence consisting of alternating diabatic and adiabatic exchange pulses. The corresponding time evolution operators in the odd parity subspace are:

$$U_{\mathrm{r}} = \mathrm{e}^{\mathrm{i}\Phi_{\mathrm{r}}}\mathrm{e}^{\mathrm{i}\theta_{\mathrm{r}}\boldsymbol{r}\cdot\boldsymbol{\sigma}} \tag{2}$$

$$U_{\mathrm{z}} = \mathrm{e}^{\mathrm{i}\Phi_{\mathrm{z}}}\mathrm{e}^{\mathrm{i}\theta_{\mathrm{z}}\hat{Z}} \tag{3}$$

for a diabatic and an adiabatic pulse respectively (see Supplementary Note 4: two-qubit gate simulations). Here $\boldsymbol{\sigma} = (\hat{X}, \hat{Y}, \hat{Z})$ is the vector consisting of the Pauli matrices, $\Phi_{\mathrm{r,z}} = Jt_{\mathrm{r,z}}/2$ the accumulated entangling phase during the pulse, and $\theta_{\mathrm{r,z}} = t_{\mathrm{r,z}}\sqrt{J^2 + \Delta E_z^2}/2$ the angle of rotation. The condition for a SWAP gate is $U_{\mathrm{tot}} = U_{\mathrm{r}}U_{\mathrm{z}}U_{\mathrm{r}}U_{\mathrm{z}_2}U_{\mathrm{r}_2}\cdots \equiv \hat{X}$. The number of necessary pulses depends on the angle of rotation; obviously a minimal pulse sequence requires $|\Delta E_z| \leq J$. In the typical regime of operation for devices with micromagnets, where $J < \Delta E_z$, a multi-step sequence is required. In the limit $J \ll \Delta E_z$ many steps are necessary and the pulse sequence becomes gradually an ac signal giving rise to the ac-SWAP gate[20]. Furthermore, it is essential to include the global phase which corresponds to a conditional phase evolution in the full two-qubit space and needs to vanish when implementing a SWAP gate. This protocol is highly versatile and can also produce maximally entangling gates, i.e., $\sqrt{\mathrm{SWAP}}$ if $U_{\mathrm{tot}} \equiv \mathrm{i}\hat{X}/2$ and iSWAP for $U_{\mathrm{tot}} \equiv \mathrm{i}\hat{X}$. While finding an optimal sequence for such a composition can be done in general following the procedure of ref. [32], here we extend these considerations into a multi-qubit space, which gives rise to additional constraints.

A possible minimal length solution for a SWAP gate is sketched in Fig. 3e and the trajectory of the qubit state is seen in the inset. In the experiment, we calibrate the exchange interaction at all stages of the pulse, fix the time of the diabatic pulses to 12 ns, and sweep the length of the adiabatic pulse t_{corr} in order to find the best point. Figure 3f shows how the four spin probabilities change when sweeping t_{corr}. We find an optimal $t_{\mathrm{corr}} = 62$ ns and the four spin state probabilities for a total pulse duration $t_{\mathrm{SWAP}} = 88$ ns are plotted in Fig. 3g. The SWAP probability exceeds 90%, where the remaining error is dominated by miscalibrations, inaccuracies in the gates needed to reconstruct

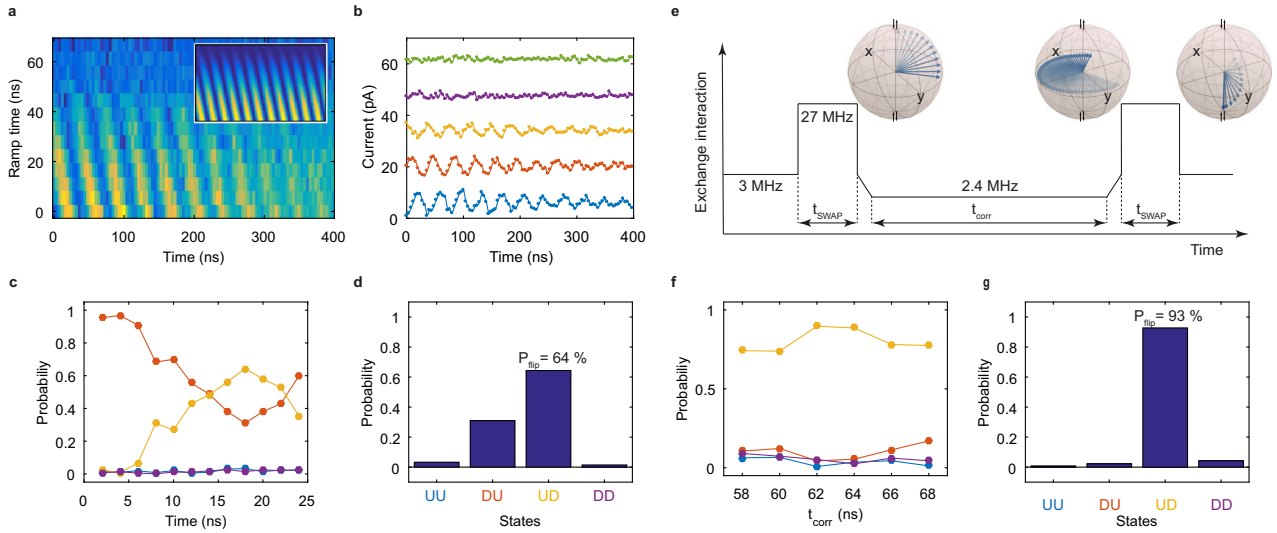

Fig. 3 Pulsed SWAP and composite exchange pulse for high-fidelity SWAP at $T = 1.05$ K. a, **b** SWAP oscillations as a function of the ramp time for a detuning pulse such that $J = 23$ MHz. When the pulsing becomes adiabatic with respect to variations in J, the exchange oscillations are suppressed. In order to maximize the readout signal we project the $|\uparrow\downarrow\rangle$ to the $|\uparrow\uparrow\rangle$ with a π pulse on f_2. Traces in **b** correspond to ramp times 0, 16, 33, 49, and 67 ns. We do not consider in these timings the finite bandwidth of the setup. Each trace has been offset by 15 pA for clarity. **c**, **d** Probabilities of the four spin states as a function of the SWAP interaction time. The states $|\uparrow\uparrow\rangle$ and $|\downarrow\downarrow\rangle$ are not affected, while the states $|\downarrow\uparrow\rangle$ and $|\uparrow\downarrow\rangle$ oscillate. Due to the finite Zeeman difference we achieve a maximum $|\uparrow\downarrow\rangle$ state probability of 64% for $t_{SWAP} = 18$ ns. The exchange interaction is set to $J = 27$ MHz. **e** Pulse sequence of the composite SWAP gate to correct for errors coming from the finite Zeeman energy difference. The Bloch spheres on top show the time evolution when starting in the $|\downarrow\uparrow\rangle$ state, with the Bloch vector depicted in nanosecond time steps. We first diabatically pulse the exchange to $J = 27$ MHz, in order to bring the state on the equator of the singlet-triplet Bloch sphere. Then we correct for the phase offset with an adiabatic exchange pulse to $J = 2.4$ MHz. We complete the state flip with another exchange pulse to $J = 27$ MHz. **f** Spin state probability after applying the composite SWAP and as a function of the adiabatic pulse time t_{corr}, from which we find the optimum $t_{corr} = 62$ ns. **g** Spin state probability after executing the composite SWAP sequence starting from the initial state $|\downarrow\uparrow\rangle$. Compared to the detuning pulse as shown in **d** we find a clear improvement in the spin flip SWAP probability.

the spin state probabilities, and state-preparation-and-measurement (SPAM) errors. We note here that constructing a SWAP gate out of CPHASEs and CROTs would result in a gate time significantly slower than the sequence discussed here. A SWAP gate can be compiled using 3 consecutive CROT gates, which would give a total SWAP time of ≈2 µs. A SWAP gate compiled from the much faster CPHASE gate requires 11 primitive operations[33], which include 8 single-qubit gates and would therefore give an even larger overhead. Therefore, the composite exchange sequence can improve the gate time by more than one order of magnitude.

Hot two-qubit gate performance. In order to assess the performance of our two-qubit gates, we perform time dependent simulations of the Heisenberg hamiltonian, based on the exchange-detuning curve that me measure experimentally (see Supplementary Note 3: Exchange spectrum). Additionally, we also take into account the effects of the finite bandwidth of the setup (300 MHz) on the pulse generation. Table 1 shows the fidelities associated with the two-qubit gates CROT, CPHASE, and SWAP. Here, F_{ideal} represents the simulated fidelities taking into account the relevant parameters, but neglecting any decoherence. We find $F_{ideal} > 99\%$ for all gates except the SWAP, which is limited in fidelity by the finite ΔE_z. At the elevated temperatures discussed in this work, thermal noise can impact the gate performances in the form of a larger charge noise amplitude[27], which couple to the spin as an effective magnetic noise via the exchange interaction. Therefore, we have also modeled the decoherence by adding stochastic fluctuations of the detuning, sampled from a $1/f$ noise spectrum (see Supplementary Note 4: Two-qubit gate simulations). By fitting the experimental data in Fig. 2b, e, we conclude that our model is able to reproduce the decoherence with good agreement. Based on these simulations we determine F_{noise}. The fidelity of the CROT and the CPHASE gate are significantly affected by the noise, due to the relatively long gate times, and we find that the predicted CROT fidelity $F_{noise} = 89\%$ is close to the experimentally measured fidelity $F = 86\%$[19]. The SWAP, diabatic CPHASE, and composite SWAP are less affected by the noise, and in particular, we predict that both the diabatic CPHASE and composite SWAP can be executed with fidelities above 99%. While experimental data will be needed to validate these predictions, these results showcases how a multitude of native two-qubit gates can be executed with high-fidelities and remarkable gate speeds. The limiting factor to the fidelities is the charge noise, as we have to significantly pulse the detuning to control the exchange interaction. Significant improvements can be expected by keeping the detuning at zero and instead pulsing

Table 1 Gate times and simulated fidelities for silicon qubits at $T = 1.05$ K.

	Gate time (ns)	F_{ideal}(%)	F_{noise}(%)
CROT	660	99.4	89.0
CPHASE	152	99.9	97.8
Diabatic CPHASE	67	99.9	99.4
SWAP	19	84.3	84.2
Composite SWAP	89	99.9	99.4

Gate times and simulated fidelities for all the two-qubit gates discussed in the main text, where F_{ideal} represents the fidelity in the absence of noise and F_{noise} takes into account the experimental noise at 1.05 Kelvin. We find high-fidelity two-qubit gates can be obtained in silicon above one Kelvin, by using diabatic CPHASE or composite SWAP sequences. The CROT fidelity is calculated as a conditional π-flip for better comparison. Good agreement is obtained with previous experiments[19], confirming that the simulated noise is an accurate estimate of the real noise. Further improvement in the fidelities of the CROT and the CPHASE may be obtained by incorporating pulse shaping[34–38].

the tunnel coupling, as this scheme is to first order insensitive to charge noise.

The ability to execute a diverse set of high-fidelity two-qubit gates define silicon quantum dots as a versatile platform for quantum information. The low magnetic field operation and the small Zeeman energy difference between qubits is furthermore beneficial for the realization of scalable qubit tiles, as it supports high-fidelity shuttlers and on-chip resonators for long-distance qubit links. Moreover, the ability to execute quantum logic at temperatures exceeding one Kelvin provides a pathway to quantum integrated circuits that host both the qubits and their control circuitry for scalable quantum hardware.

Methods

The experiments have been performed in a Bluefors refrigerator with a base temperature $T_{base} \approx 0.45$ K with a 3 Tesla magnet. In the experiments we make use of d.c. voltages and a.c. voltages. The d.c. voltages are supplied via battery-powered voltage sources and filtered through Cu-powder filters and 30 Hz and 150 kHz filters. The a.c. voltages are supplied through a bias-tee that is on the sample printed circuit board with a cut-off frequency of 3 Hz. Pulses are generated by an arbitrary wave form generator (Keysigh M3202A) with 14 bit resolution and 1 GS/s. Microwave signals are applied via a Keysight E8267D.

Data availability

The measurement and analysis code and the underlying data is available in the Zenodo repositories (10.5281/zenodo.7179960).

Received: 4 March 2021; Accepted: 11 October 2022;
Published online: 02 November 2022

References

1. Arute, F. et al. Quantum supremacy using a programmable superconducting processor. *Nature* **574**, 505–510 (2019).
2. Reiher, M., Wiebe, N., Svore, K. M., Wecker, D. & Troyer, M. Elucidating reaction mechanisms on quantum computers. *Proc. Natl Acad. Sci. USA* **114**, 7555–7560 (2017).
3. Ladd, T. D. et al. Quantum computers. *Nature* **464**, 45–53 (2010).
4. Loss, D. & DiVincenzo, D. P. Quantum computation with quantum dots. *Phys. Rev. A* **57**, 120–126 (1998).
5. Petta, J. R. et al. Coherent manipulation of coupled electron spins in semiconductor quantum dots. *Science* **309**, 2180–2184 (2005).
6. He, Y. et al. A two-qubit gate between phosphorus donor electrons in silicon. *Nature* **571**, 371–375 (2019).
7. Meunier, T., Calado, V. E. & Vandersypen, L. M. K. Efficient controlled-phase gate for single-spin qubits in quantum dots. *Phys. Rev. B* **83**, 121403 (2011).
8. Nowack, K. C., Koppens, F., Nazarov, Y. V. & Vandersypen, L. Coherent control of a single electron spin with electric fields. *Science* **318**, 1430–1433 (2007).
9. Veldhorst, M. et al. An addressable quantum dot qubit with fault-tolerant control-fidelity. *Nat. Nanotechnol.* **9**, 981–985 (2014).
10. Kawakami, E. et al. Electrical control of a long-lived spin qubit in a Si/SiGe quantum dot. *Nat. Nanotechnol.* **9**, 666–670 (2014).
11. Yoneda, J. et al. A quantum-dot spin qubit with coherence limited by charge noise and fidelity higher than 99.9%. *Nat. Nanotechnol.* **13**, 102 (2018).
12. Veldhorst, M. et al. A two-qubit logic gate in silicon. *Nature* **526**, 410–414 (2015).
13. Watson, T. F. et al. A programmable two-qubit quantum processor in silicon. *Nature* **555**, 633–637 (2018).
14. Xue, X. et al. Benchmarking gate fidelities in a Si/SiGe two-qubit device. *Phys. Rev. X* **9**, 021011 (2019).
15. Zajac, D. M. et al. Resonantly driven CNOT gate for electron spins. *Science* **359**, 439–442 (2018).
16. Huang, W. et al. Fidelity benchmarks for two-qubit gates in silicon. *Nature* **569**, 532–536 (2019).
17. Hendrickx, N. W., Franke, D. P., Sammak, A., Scappucci, G. & Veldhorst, M. Fast two-qubit logic with holes in germanium. *Nature* **577**, 487–491 (2020).
18. Yang, C. H. et al. Operation of a silicon quantum processor unit cell above one kelvin. *Nature* **580**, 350–354 (2020).
19. Petit, L. et al. Universal quantum logic in hot silicon qubits. *Nature* **580**, 355–359 (2020).
20. Sigillito, A. J., Gullans, M. J., Edge, L. F., Borselli, M. & Petta, J. R. Coherent transfer of quantum information in a silicon double quantum dot using resonant swap gates. *npj Quantum Inform.* **5**, 1–7 (2019).
21. Barenco, A. et al. Elementary gates for quantum computation. *Phys. Rev. A* **52**, 3457 (1995).
22. Veldhorst, M., Eenink, H. G. J., Yang, C. H. & Dzurak, A. S. Silicon CMOS architecture for a spin-based quantum computer. *Nat. Commun.* **8**, 1766 (2017).
23. Vandersypen, L. M. K. et al. Interfacing spin qubits in quantum dots and donors-hot, dense, and coherent. *npj Quantum Inform.* **3**, 34 (2017).
24. Li, R. et al. A crossbar network for silicon quantum dot qubits. *Sci. Adv.* **4**, eaar3960 (2018).
25. Lawrie, W. I. L. et al. Quantum dot arrays in silicon and germanium. *Appl. Phys. Lett.* **116**, 080501 (2020).
26. Urdampilleta, M. et al. Gate-based high fidelity spin read-out in a CMOS device. *Nat. Nanotechnol.* **14**, 737–741 (2019).
27. Petit, L. et al. Spin lifetime and charge noise in hot silicon quantum dot qubits. *Phys. Rev. Lett.* **121**, 076801 (2018).
28. Russ, M. et al. High-fidelity quantum gates in Si/SiGe double quantum dots. *Phys. Rev. B* **97**, 085421 (2018).
29. Burkard, G., Loss, D., DiVincenzo, D. P. & Smolin, J. A. Physical optimization of quantum error correction circuits. *Phys. Rev. B* **60**, 11404 (1999).
30. Maune, B. M. et al. Coherent singlet-triplet oscillations in a silicon-based double quantum dot. *Nature* **481**, 344 (2012).
31. Vandersypen, L. M. K. & Chuang, I. L. Nmr techniques for quantum control and computation. *Rev. Mod. Phys.* **76**, 1037 (2005).
32. Zhang, X.-M., Li, J., Wang, X. & Yung, M.-H. Minimal nonorthogonal gate decomposition for qubits with limited control. *Phys. Rev. A* **99**, 052339 (2019).
33. Lee, S. et al. The cost of quantum gate primitives. *J. Multiple-Valued Logic Soft Comput.* **12**, 561–573 (2006).
34. Martinis, J. M. & Geller, M. R. Fast adiabatic qubit gates using only σ z control. *Phys. Rev. A* **90**, 022307 (2014).
35. Güngördü, U. & Kestner, J. Pulse sequence designed for robust c-phase gates in simos and si/sige double quantum dots. *Phys. Rev. B* **98**, 165301 (2018).
36. Calderon-Vargas, F. et al. Fast high-fidelity entangling gates for spin qubits in si double quantum dots. *Phys. Rev. B* **100**, 035304 (2019).
37. Güngördü, U. & Kestner, J. Analytically parametrized solutions for robust quantum control using smooth pulses. *Phys. Rev. A* **100**, 062310 (2019).
38. Güngördü, U. & Kestner, J. Robust implementation of quantum gates despite always-on exchange coupling in silicon double quantum dots. *Phys. Rev. B* **101**, 155301 (2020).

Acknowledgements

We thank S. de Snoo and S.G.J. Philips for software developments and the Veldhorst group for useful discussions. M.V. acknowledges support through a Vidi and an NWO grant, both associated with the Netherlands Organization of Scientific Research (NWO). Research was sponsored by the Army Research Office (ARO) and was accomplished under Grant No. W911NF- 17-1-0274. The views and conclusions contained in this document are those of the authors and should not be interpreted as representing the official policies, either expressed or implied, of the Army Research Office (ARO), or the U.S. Government. The U.S. Government is authorized to reproduce and distribute reprints for Government purposes notwithstanding any copyright notation herein.

Author contributions

L.P. performed the experiments, M.R. developed the theoretical models. H.G.J.E. and W.I.L.L. were responsible for the device fabrication. J.S.C. supervised the wafer growth. L.P. and M.R. analyzed the data with input from L.M.K.V. and M.V. L.P., M.R., and M.V. wrote the manuscript with input from all authors. M.V. conceived and supervised the project.

Competing interests

The authors declare no competing interests.

Additional information

Supplementary information The online version contains supplementary material available at https://doi.org/10.1038/s43246-022-00304-9.

Correspondence and requests for materials should be addressed to Menno Veldhorst.

Peer review information *Communications Materials* thanks the anonymous reviewers for their contribution to the peer review of this work. Primary Handling Editors: Aldo Isidori.

Reprints and permission information is available at http://www.nature.com/reprints

Publisher's note Springer Nature remains neutral with regard to jurisdictional claims in published maps and institutional affiliations.